Journal of Thermal Analysis and Calorimetry, Vol. 82 (2005) 565–574

CAN ONE MEASURE PRECISE HEAT CAPACITIES WITH DSC OR TMDSC?
A study of the baseline and heat-flow rate correction

J. Pak, W. Qiu, M. Pyda, E. Nowak-Pyda and B. Wunderlich[*]

Department of Chemistry, The University of Tennessee, Knoxville, TN 37996-1600, and
Chemical Sciences Division, Oak Ridge National Lab., Oak Ridge, TN 37831-6197, USA

During a prior study of gel-spun fibers of ultrahigh-molar-mass polyethylene, a substantial error was observed on calculating the heat capacity with a deformed pan, caused by the lateral expansion of the fibers on shrinking during fusion. In this paper, the causes of this and other effects that limit the precision of heat capacity measurements by DSC and TMDSC are explored. It is shown that the major cause of error in the DSC is not a change in thermal resistance due to the limited contact of the fibers with the pan or the deformed pan with the platform, but a change in the baseline. In TMDSC, the frequency-dependence is changed. Since irreversible changes in the baseline can occur also for other reasons, inspections of the pan after the measurement are necessary for precision measurements.

Keywords: *baseline, DSC, heat capacity, instrument lag, precision, thermal resistance, TMDSC*

Introduction

The determination of heat capacity has been the main goal in our laboratory for 50 years. This objective was pursued with classical and scanning adiabatic calorimetry [1], differential thermal analysis, DTA [2, 3], and later with differential scanning calorimetry, DSC [4, 5]. The introduction of computers for data handling and analysis increased the precision to better than 1% [6]. More recently, temperature-modulated differential scanning calorimetry, TMDSC, became available and seemed to have great promise [7]. After detailed study of the new methods, considerable progress was reached when using multi-frequency analysis. A precision approaching 0.1% could be demonstrated with all three major commercial DSCs [8–10]. Over the years these improvements have led to a critical collection of tables of heat capacities for about 200 macromolecules and related compounds [11]. The value of such data was proven by the quantitative link of thermal properties to molecular motion which allowed the characterization of different phases of importance to describe the change of properties of the polymers during synthesis, processing, and aging [12, 13].

All analyses discussed operate by scanning of temperature in an approximately isothermal surroundings, in isoperibol calorimeters [14]. The measured heat-flow rates must in these cases be corrected with separately evaluated baselines. When only qualitative information is looked for, or rather large latent heats need to be determined, as for first-order phase transitions and chemical reactions, a common practice is to combine the baseline with the effect of the thermodynamic heat capacity, C_p. Then, the combined baseline accounts for both, the asymmetry of heat losses and the heat capacity, $C_p=(\partial H/\partial T)_{n,p}$ which represents the change in heat content, H, with temperature, T, at constant composition, n, and pressure, p. This qualitative solution also reduces the precision of the latent heat for broad transitions, and, naturally, excludes the measurement of heat capacity.

Experimental

Instrumentation

A Thermal Analyst 2920® system from TA Instruments was used for TMDSC with an underlying heating rate and all standard DSC measurements. For complex saw-tooth modulation for simultaneous, multi-frequency TMDSC, a TA Instruments, Inc. DSC Q1000™ was programmed in the standard DSC mode of operation. Both calorimeters are isoperibol, twin-heat-flux calorimeters with modulation control at the sample-temperature sensor. The indicated temperatures of the equipment were checked in the standard DSC mode with the onset of melting of indium (429.75 K) and water (273.15 K) at scanning rates of 10 K min^{-1}, determined by extrapolating the linear portion of the melting peak to the baseline. The

* Author for correspondence: athas@utk.edu

1388–6150/$20.00
© 2005 Akadémiai Kiadó, Budapest
Akadémiai Kiadó, Budapest, Hungary
Springer, Dordrecht, The Netherlands

heat-flow rate was initially calibrated with the heat of fusion of indium (28.62 J g^{-1}).

For the 2920® system, dry N_2 gas was purged through the DSC cells with a flow rate of 25 mL min^{-1} and also at variable rates, as indicated in the specific experiment descriptions. Cooling was accomplished with a refrigerated cooling system. The baseline without pans of the DSC is shown in Fig. 1 as curve A. In the temperature range of interest, the asymmetry of the baseline is close to 0.1 mW, too much, not to be corrected for. In all runs for higher precision, thus, the asymmetry was determined with a run using an empty pan on each platform. For heat capacity measurements, further corrections were made with calibration runs using an Al_2O_3 single crystal disc (sapphire) of 22.564 mg. The empty reference pan was the same for all runs and had a mass of 22.370 mg.

For the Q1000® system, dry N_2 gas was purged through the DSC cell with a flow rate of 10 mL min^{-1}. Cooling was accomplished with a refrigerated cooling system having a capacity to reach 185 K. For the complex saw-tooth modulation, the heat-flow-rate was on-line corrected with the Tzero© calibration method [15]. The drift of the baseline after the standard calibration was then less than 0.05 mW between 185 and 670 K, as is shown in Fig. 1, curve B. This precision made it unnecessary to do additional asymmetry corrections. Final heat capacity calibrations were made with 25.966 mg of sapphire, and the sample measurements were carried out with 2.629 mg of polyethylene fiber. The sample and reference pan masses were always chosen to match with about 23 mg. The Tzero©-corrected data were collected as recorded by the commercial software of the DSC. All further calculations were performed externally based on the software package of Mathematica 3.0.

Standard TMDSC with an underlying heating rate

The TMDSC was carried out with the 2920® DSC using an underlying heating rate, $\langle q \rangle$=2 K min^{-1}, a period of 60 s, and an amplitude of 0.5 K in the temperature range from 365 to 440 K. The heating run was followed by a cooling run. Thereafter, this sequence of heating and cooling was repeated two more times on the same sample. The reversing heat capacity and the phase of the heat-flow rates were obtained from these six measurements.

Simple sinusoidal modulation at different frequencies

Quasi-isothermal TMDSC [16] which uses no underlying heating rate ($\langle q \rangle$=0) was done with the 2920® DSC employing a simple sinusoidal modulation at 301.95 and 451.65 K, below and above the melting

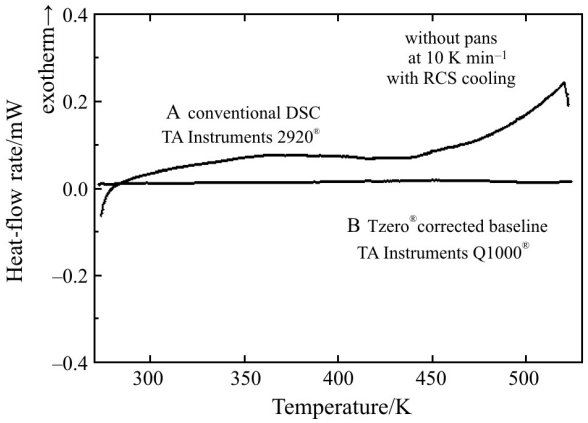

Fig. 1 Baselines indicating the asymmetry of the DSC obtained from runs without pans using the two different instruments used in this research

peak of the fiber samples. The modulation frequencies, $\omega=2\pi/p$, with periods, p=40, 60, 80 and 100 s were coupled with modulation amplitudes of 0.5 K. The heat capacity measurements were done twice for each sample (fiber, premelted fiber, and PE15520) with an empty pan and Al_2O_3 in the common sequence for the measurement of heat capacity.

Multifrequency sawtooth modulation

These experiments were carried out with the Q1000© DSC. Quasi-isothermal experiments were performed with the simplified, complex sawtooth-modulation presented in Fig. 2 by curve A. Figure 2, curve B, illustrates the response of the chosen calorimeter. A comparison with Fig. 2 in Ref. [10] illustrates the improved performance of the Q1000® relative to the 2920® DSC. Each sub-segment lasts 30 s and the harmonics are of frequencies $\nu\cdot\omega$ with with ν= 1, 3, 5, 7 and 9 corresponding to periods p of 420, 140, 84, and

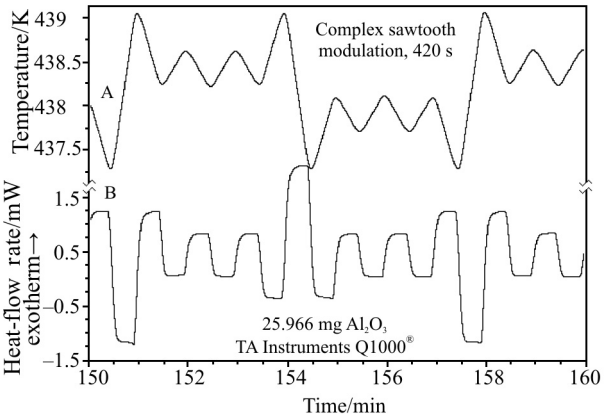

Fig. 2 Complex Sawtooth modulation to create multi-frequency modulation of similar amplitude with the harmonics of the sample temperature (A) and the heat-flow rate (B), taken from a sapphire calibration run of 25.966 mg Al_2O_3

60 and 46 $^2/_3$ s. The quasi-isothermal experiments were done at 308 and 438.15 K for Al_2O_3 and the fibers. The experiment was repeated 15 times at each temperature. In these experiments the different frequency response was tested on the identical sample at the same time, so that changes could be minimized.

Standard DSC on undeformed and deformed Al pans

These measurements with empty Al pans on both measuring positions of the 2920® DSC were made at 10 K min^{-1} by heating from 303.15 to 403.15 K with 10 min isotherms at the beginning and end of each run. The flow rate of the purge gas was changed from 5 to 75 mL min^{-1} on a series of measurements with undeformed, flat-bottom pans of 23.4 mg Al.

This was followed with several series of measurements at 25 mL min^{-1} N_2 flow on variously deformed pans with different masses. The Al pans with flat bottom were changed in mass from 23.4 to 56.1 mg by adding additional lids. One set of pans with different numbers of lids was pressed inward with a suitable plastic tool after crimping, to give the pans a concave bottom. The masses varied from 23.4 to 67.4 mg. Another set of the pans and lids was shaped outward, to be convex, and was analyzed with masses from 23.3 to 57.1 mg.

Sample description

The samples, named 'fiber', always refer to ultrahigh-molar-mass polyethylene, UHMM PE, produced as a fiber by gel spinning. The fiber was provided by Allied-Signal Inc. The polymer had a molar mass above 10^6 Da and was similar to the commercial Spectra™ 900. Its thermal properties are described in detail in Refs [17, 18] (fiber PE-III in [17]). The fibers were cut before placement into the sample pan. Its strands were untwisted and placed between a doubly folded weighing paper. The weighing paper was next taped to a board and cut with a single-edged razor into about 3 mm wide strips. The fibers were then transferred to the DSC pan with the help of the weighing paper. This procedure left the fibers largely parallel. The fibers were sealed in the standard Al pans of about 20 μL volume, and laterally compressed on crimping the sample pan.

The sample named 'premelted-fiber' was prepared by heating the UHMM PE fiber within its pan without a lid to 450 K in a separate oven. The resulting melt was pressed at this temperature to be flat within the pan. The sample pan was then sealed with a lid as usual.

The sample named 'PE15520' was purchased from Scientific Polymer Products Inc. Its mass average molar masses was 15,520 Da, and M_w/M_n was 1.08, according to information by the supplier. Its reversible melting was studied earlier [19].

Results

Phase shift of the heat-flow and the deformation of the pan on TMDSC of fiber samples

From the previous study [18], it was known that the pan deformed to a convex bottom during the melting transition on the 1st heating run, as shown in Fig. 3. Deformations to a concave bottom were seen frequently when cooling melted samples of polyesters, such as poly(butylene terephthalate). In these cases, the polymer melt wetted the crimped seal and often spread to the top of the pan, causing problems in the determination of the heat capacity. In this study, we want to explore the details when deformations occur and how the measurements are affected by it.

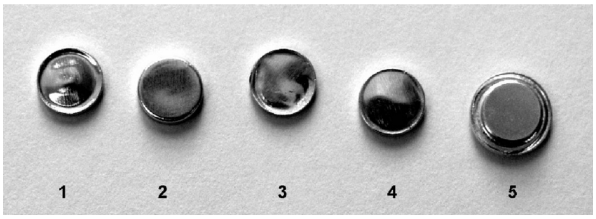

Fig. 3 Photograph of the bottom of five aluminum pans. Pan 2 is an empty pan for reference. Pans 1, 3 and 4 are filled with 2.296, 0.51 and 2.777 mg of fiber samples, respectively, photographed after completion of the melting runs. Pan 5 is the bottom of a heavier pan of about 40 mg which resists deformation

The fibers were first heated from 365 to 440 K in the TMDSC mode with an underlying heating rate of 2 K min^{-1} and cooled to 365 K with the same rate. Without removing the samples, the DSC this cycle was repeated twice. The reversing heat capacity and the phase of the heat-flow rate were obtained from these measurements. The results from 2nd and 3rd heating runs were identical. Similarly, all three cooling measurements were superimposable. Therefore, in the following figures the 1st and 2nd heating runs and 1st cooling run are depicted only. Figure 4 shows the reversing heat capacity of the fiber with the continuous thin curves. The data in Fig. 4 are not corrected for asymmetry and not calibrated with Al_2O_3. The dotted line represents the heat capacity of a 100% amorphous sample extrapolated from the melt to lower temperature, and the solid line is for the vibrational heat capacity of a 100% crystalline sample, as given in the ATHAS data bank [11–13]. The thick solid line represents the same fiber, measured by quantitative standard DSC on heating and cooling in sequences of

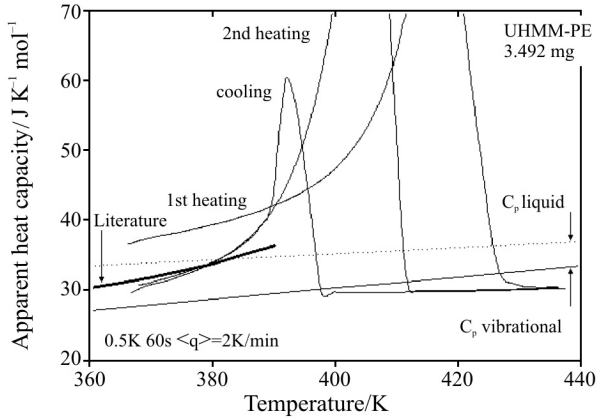

Fig. 4 Uncorrected, reversing, apparent, heat capacities of 3.492 mg of UHMM-PE gel-spun fibers measured by TMDSC with an underlying heating and cooling rate (thin lines). Prior precision data on the same sample up to the beginning of major melting are given by the thick line [17]

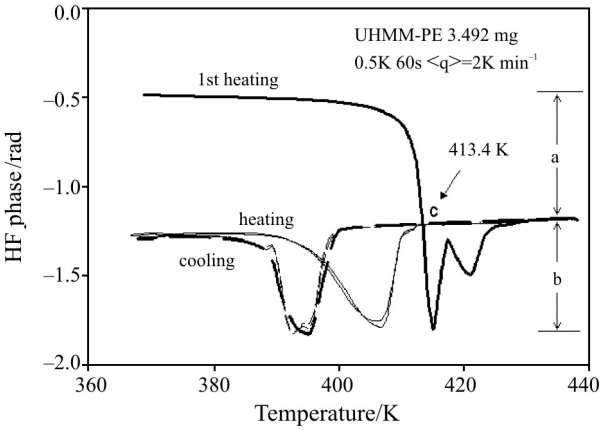

Fig. 6 Phase-shift of the heat-flow rate of the data in Fig. 5 as a function of temperature. The thick solid line is for the 1st heating and the thin continuous lines are for the 2nd and 3rd heating runs. The dashed lines are for the three cooling runs

steps of 10 K at 10 K min^{-1}, interrupted by isotherms in overlapping sequences from 173 to 403 K [17].

In Fig. 5, the uncorrected data in the low-temperature region on first heating were calibrated internally to the heat capacity below the melting region available in the literature [17]. For small sample masses this calibration process yields better results than a separate run with Al_2O_3 for calibration. In the case of the fiber analysis, a small sample mass was chosen to minimize the pressure effect caused by the shrinkage of the fibers on the phase transitions within the fibers [17]. Typical masses required for the measurement of absolute heat capacities of polymers linked to the C_p of Al_2O_3 are usually 15–30 mg [3]. The data of Fig. 5 up to the melting peak of the first heating are now of good precision. The heat capacity of the melt, as well as the data found on the subsequent cooling and heating, however, are unacceptable. All these unacceptable data after the first melting are reproducible for the subsequent heating and cooling experiments.

Figure 6 shows the changes of the phase shift of the reversing heat-flow-rate measurement (HF) as a function of temperature, and Fig. 7 illustrates the same data as a function of time. A drastic change is observed during the 1st heating run. Before the melting, the heat-flow-rate phase difference is –0.5 rad, and after the transition, it is –1.2 rad. After cooling, it does not return to the original value. The 2nd and 3rd heating and cooling runs are reproducible without further irreversible phase shifts. We conclude that before the melting transition, the heat-flow- rate-phase difference is about –0.5 rad with a flat bottom pan, as shown in Fig. 3(2). With a deformed pan, similar to Fig. 3(4), the heat-flow-rate-phase difference is about –1.3 rad.

From these results, it is obvious that the data must be evaluated separately before and after the shift

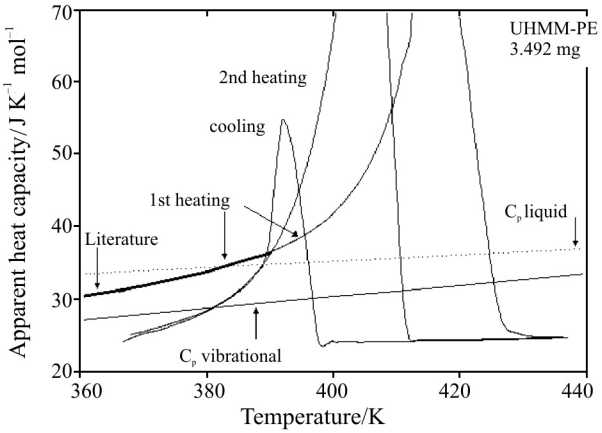

Fig. 5 Reversing, apparent heat capacities of UHMM-PE gel-spun fibers as in Fig. 5, but corrected to the literature data at low-temperatures on first heating [17]

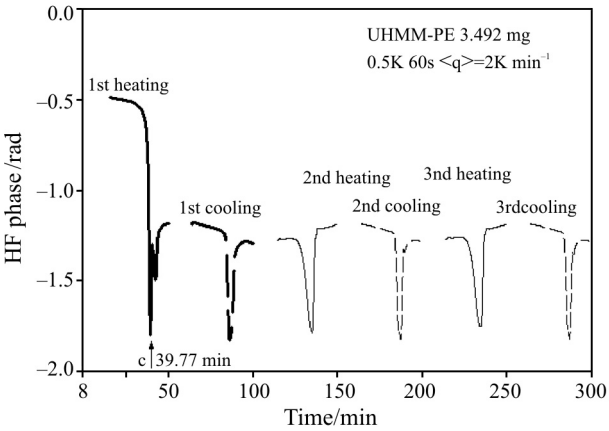

Fig. 7 Phase-shift as in Fig. 6, but plotted as a function of time, clearly indicating the deformation of the pan at point c, corresponding to 413.4 K

of the phase difference of the heat-flow rate to obtain the correct values of the heat capacity. The amount 'a' in Fig. 6 is the shift of the phase of the heat-flow rate due to the pan deformation and the amount 'b' is due to the transitions which is identical for all melting as well as crystallization transitions. Therefore, on the first heating run at 413.4 K in Fig. 6 or 38.25 min in Fig. 7, the initial low-temperature baseline is shifted to the new phase-difference of –1.3 rad with a deformed pan. This point is marked 'c' in Figs 6 and 7. For a proper calibration, C_p before point 'c' must be shifted downward by 5.64 J K mol^{-1} and after 'c,' it is to be shifted up by 12.10 J K mol^{-1}. Figure 8 illustrates good agreement with the ATHAS Data Bank of the C_p of the liquid polyethylene [11], as well as the literature data of the fibers [17] when correcting twice, as suggested by Fig. 6.

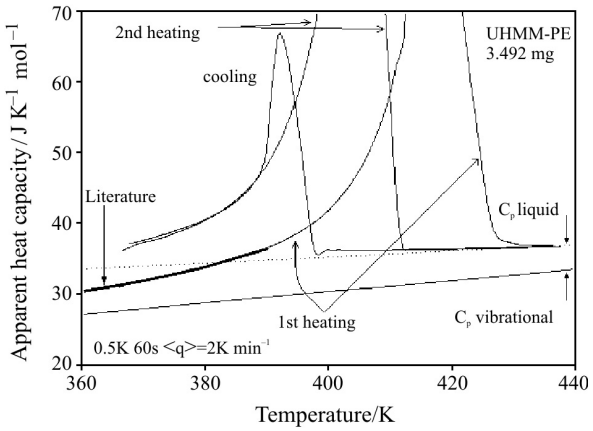

Fig. 8 Apparent, reversing heat capacities of 3.492 mg UHMM-PE as in Fig. 4, but fitted to the known heat capacity of the solid state at low-temperature, and to the known heat capacity of the liquid state at high-temperature

Frequency dependence of heat capacity when using sinusoidal temperature modulation

To establish the effect of a deformed pan on TMDSC, measurements with different frequencies were made. One commonly evaluates the reversing heat capacity from the equations:

$$C_p = \frac{A_{HF}}{A_{T_S}\omega} K(\omega); \quad K(\omega) = \sqrt{1+\tau^2\omega^2} \qquad (1)$$

where ω is the frequency (=2π/p), K(ω) is a frequency-dependent calibration factor, and τ is a correction factor when analyzing the heat capacity at different frequencies. Under the usual conditions of continued steady state, linearity, and stationarity of response, τ is a constant (=C_r /K, where C_r is the heat capacity of the empty reference pan and K is the Newton's law constant of the DSC) [7]. At higher frequencies, τ becomes frequency dependent [20] and has to be calibrated for every calorimeter configuration.

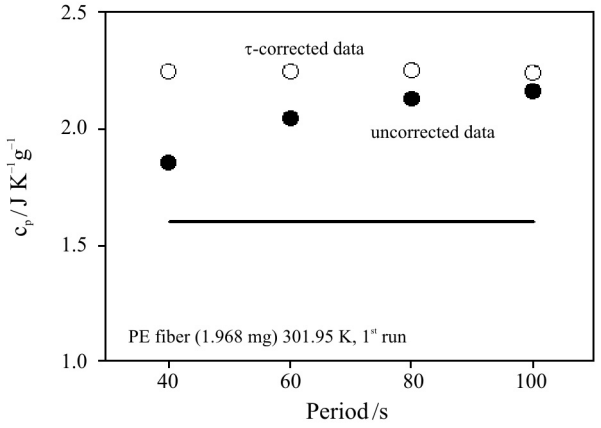

Fig. 9 Specific heat capacity of the fiber on the 1st run (no pan deformation) for separate sinusoidal modulation with p of 40 to 100 s. Filled circles, (●), uncorrected heat capacities calculated using Eq. (1) with K(ω)=1. Open circles, (❍), corrected according to Eq. (1) with τ from the linear fitting in Fig. 10. The solid line is taken from the ATHAS Data Bank for the vibrational heat capacity of the solid

Figure 9 displays the 1st measurement at 301.95 K on a fresh sample of the fiber. The uncorrected heat capacities (●) increase with increasing period, p. The value of τ is constant when evaluated from the slope of the line representing the uncorrected data in Fig. 10. The open circles (❍) in Fig. 9 are the corrected heat capacities with the given τ. To compare with the solid line of the vibrational heat capacity of the crystal, the calibration with Al_2O_3 would have to be done, in addition to corrections for the increase in heat capacity originating from the mobile fraction and the trans-gauche contribution from the heat capacity of the crystals [17]. During this part of

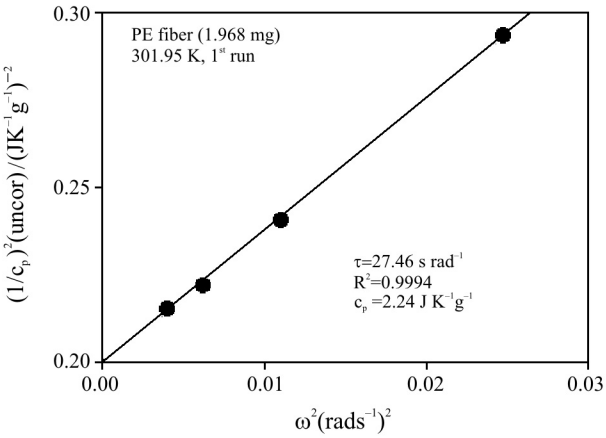

Fig. 10 Square of the inverse, uncorrected specific heat capacity of the fiber (● in Fig. 9) plotted as a function of the square of the modulation frequencies

the run, the pan is not deformed, as presented in Fig. 3(2), and a proper value of τ has been found.

Next, the sample is heated up to 450.65 K, above the melting temperature of the fibers. The pan is now deformed, as shown in Fig. 3 (3 or 4), having passed through the melting transition at about 420 K. The uncorrected heat capacities now decrease with the period instead of showing an increase. This behavior is surprising and inconsistent with a simple change in thermal resistance, as one might think is happening on deformation of the pan.

Cooling the fiber after melting to 301.95 K for the 2nd run leads to the data of Figs 11 and 12. The uncorrected heat capacities still behave as they did at the higher temperature. The abnormal behavior of τ, thus, is linked to the deformation of the pan and not due to changes of state of the sample. The subsequent heatings and coolings cause no further changes in the behavior of τ, the higher frequency measurements lead to erroneously higher heat capacities.

The same experiments were done for comparison with two other PE samples. One is of the premelted fiber (3.318 mg), the other is with PE15520 (5.630 mg), both are described in the experimental section. During their melting transitions, the pans did not deform and τ was constant over the whole frequency range used, as in Fig. 9. The results are summarized in Table 1. The trends in τ, as far as could be measured, are as expected. The larger the sample mass, the larger is τ, and the higher the temperature, the lower is τ. The low-temperature data of the second runs are expected to have better packed samples after melting and show a lower τ. The high-temperature data of the first and second runs refer to practically the same melts, and the values of τ are practically equal.

These results lead, however, to a new question. Why do the uncorrected heat capacities decrease as the modulation period increases when the measurements are done with deformed pans, as shown in Fig. 11. To answer this question, the amplitudes in the semicrystalline state at different frequencies are compared before and after the deformation. The data are summarized in Table 2. The amplitudes of the heat-flow rate decrease in the 1st run by 56% with decreasing frequency, while in the 2nd run by 74%, when measuring with the deformed pan, while the product

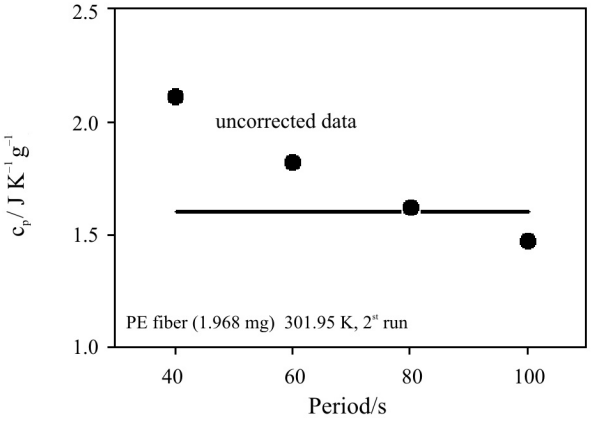

Fig. 11 Specific heat capacity of the fiber on the 2nd heating run. Conditions as in Fig. 9, but now with a deformed

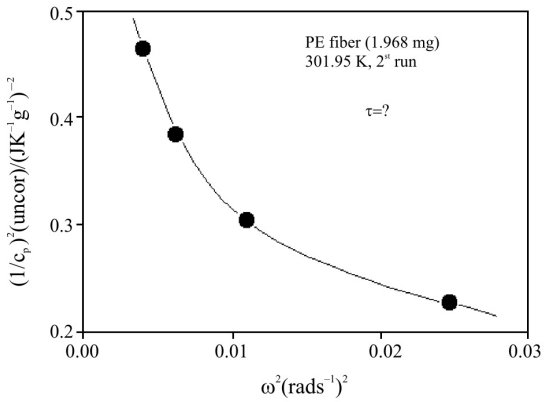

Fig. 12 Square of the inverse, uncorrected specific heat capacity of the fiber (● in Fig. 11) plotted as a function of the square of the modulation frequencies

A_{Ts}·T stays the same, i.e., follows the chosen modulation cycles, as expected. Taking the ratio, as suggested in Eq. (1), the heat capacity decreases with frequency in the first run, as expected, but increases in the second, after the deformation of the pan. It is also noted, that the heat-flow-rate amplitude for the deformed pan is higher at high frequency and lower at low frequency.

To check the shape of the heat-flow-rate curve, a Fourier-transform was done up to the 9th harmonic. The data for a period of 60 s are given in Table 3 as an example. The amplitude of the response comes mainly from 1st harmonic and the higher harmonics have less than 0.1% contribution for all measurements with different periods from 40 to 100 s. As a result, the shape of the

Table 1 The τ values for different samples

Sample	τ on the 1st run /s rad^{-1}		τ on the 2nd run /s rad^{-1}	
	301.95 K	451.65 K	301.95 K	451.65 K
Fiber[a]	27.46	NA	NA	NA
Premelted Fiber[b]	31.87	27.36	29.95	27.37
PE15520[c]	36.70	28.65	34.04	28.91

[a–c] The sample masses were 1.968, 3.318, and 5.630 mg, respectively

Table 2 Amplitudes of the heat-flow rate and the rate of temperature-change of the first harmonic

at 301.95 K	A_{HF} /mW		$A_{Ts}\omega$ K rad s^{-1}	
period /s	1st run	2nd run	1st run	2nd run
40	0.3362	0.3754	0.0785	0.0784
60	0.2308	0.2070	0.0523	0.0523
80	0.1758	0.1348	0.0393	0.0392
100	0.1496	0.0979	0.0323	0.0316

Table 3 Heat-flow-rate amplitude for higher harmonics of the Fourier series

p=60 s at 301.95 K	heat-flow-rate amplitude/mW	
# of the harmonic	1st run	2nd run
amplitudes as read from the raw data	0.2310	0.2080
1	0.2308	0.2070
2	0.0012	0.0016
3	0.0002	0.0003
5	0.0002	0.0001
7	0.0001	0.0003
9	0.0002	0.0001

heat-flow-rate signal is close to a perfect sine curve and cannot cause the increase in C_p with frequency.

Values for τ from complex sawtooth modulation

The TMDSC with a complex sawtooth modulation using the Q1000®, as shown in Fig. 2 was done to make certain that an identical sample and pan configuration is analyzed at all frequencies. The amplitudes of the heat-flow rate for each harmonic frequency νω, $A_{HF}(\nu)$, and the corresponding sample-temperature amplitudes, $A_{Ts}(\nu)$, were inserted into Eq. (1). The time constant τ can then be obtained, as before, by plotting the inverse of the squared, uncorrected heat capacity *vs.* the square of the frequency. The intercept of the plot at $(\nu\omega)^2=0$ is the inverse of the squared, τ-corrected heat capacity [20]. The final step in the analysis is the evaluation of the correction factor from the preliminary setting of the heat flow from the indium heat of fusion by comparison with a sapphire experiment. It should be noted that with the Tzero® online asymmetry correction a separate run with two empty pans is not required, as can be seen from Fig. 1. For the longest modulation periods, p, the τ-correction becomes negligible. The complex sawtooth shown in Fig. 2 was designed to have close to the same amplitudes at the 1st, 3rd, 5th, and 7th harmonic. The 9th harmonic was not originally included in the analysis and has a smaller amplitude, but it is still measurable because it combines residual contributions from several harmonics of the other sawtooth components.

Figure 13 illustrates that before melting, the uncorrected heat capacities of the fiber sample increases as the period increases, as expected and yields at low frequency a linear relationship between the inverse of the squared, uncorrected heat capacities and the square of the frequencies. The value of τ is derived to be 12.9 s rad^{-1} from the slope. Above the melting temperature, in contrast, the pan was deformed, as shown in Fig. 3(1) and as before, a value of τ could not be evaluated. The heat capacities shown in Fig. 14 are obtained on the second heating of the sample. As in Fig. 11, the C_p decreases with period, yielding as for the melt, no value for τ.

Standard DSC on undeformed and deformed aluminum pans

To evaluate the effect of the flow rate of the purge gas, heat-flow rates were measured as a function of time with an empty sample pan with a flat bottom as shown in Fig. 3(2). From 5–50 mL min^{-1} of N_2 flow rates, steady state was reached approximately three minutes after the start of heating. At higher gas-flow rates, steady state was reached later, reaching seven minutes at 75 mL min^{-1}. At steady state, the heat-flow rates were not dependent on the gas-flow rate. The initial isotherm was constant for all runs at a heat-flow rate of –0.110±0.009 mW. The final isotherm gave, similarly, –0.159±0.010 mW, and during heating at

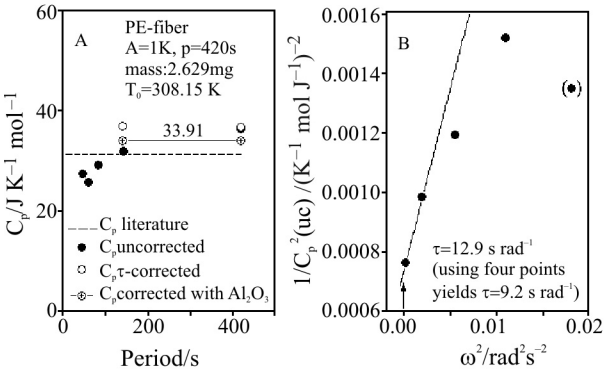

Fig. 13 Quasi-isothermal analysis of UHMM gel-spun polyethylene fibers with a complex sawtooth modulation as shown in Fig. 2. Run at 308.15 K, below the first melting. The plot on the right shows the evaluation of the ●-value as given by Eq. (1)

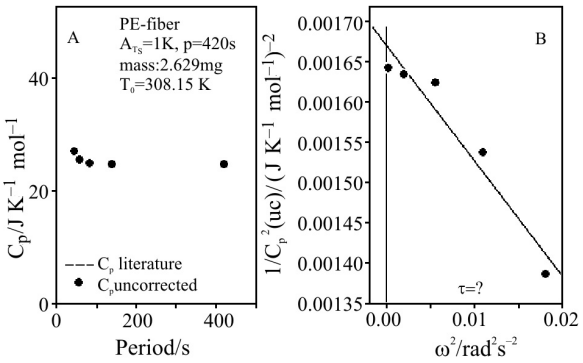

Fig. 14 Quasi-isothermal analysis of UHMM gel-spun polyethylene fibers with a complex sawtooth modulation as shown in Fig. 2. Run at 438.15 K, in the melting region. The plot on the right shows that no evaluation of the τ-value is reasonable

353.15 K, the asymmetry reached –0.438±0.016 mW. For subsequent experiments, the flow rate was set to 25 mL min^{-1} which seemed to be most reproducible.

Figure 15 gives the DSC results of measurements of sample pans with flat and deformed bottoms with changing mass. The pan mass causes an increase in the heat-flow rate that is close-to linear and for the series of measurements with flat bottoms it is similar to the known heat capacity of Al. Note that the deformed pan with a concave bottom shows a positive heat-flow rate (asymmetry) at a lower pan mass which changes only to a negative signal when the sample pan is twice as heavy as the reference pan. The convex pan shows less of a change in the positive heat-flow rate. The average lines through the convex and concave pans of Fig. 15 yield lower heat capacities, as can be seen from the smaller slopes.

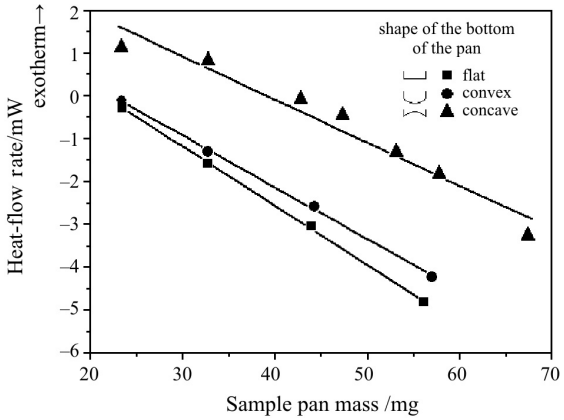

Fig. 15 Heat-flow rates as a function of pan mass for differently shaped sample pans

Discussion

Based on the theoretical model of Ozawa [21], the proper handling of the baseline for heat capacity measurements with standard DSC was derived some time ago and has been summarized repeatedly [3]. Three runs need to be performed, an asymmetry correction (empty pan *vs*. identical empty pan), the measurement proper (sample within pan *vs*. identical empty pan) and a calibration run (reference sapphire within pan *vs*. identical empty pan). First, the isotherms of all runs must be inspected. They should agree for the three runs, or must be corrected by a parallel shift to the heat-flow-rate axis. If this cannot be achieved, the runs must be discarded because of changes in the calorimeters during the runs. The proper asymmetry correction can only be made after steady state has been reached for all three experiments. The missing time where no data should be collected must be made up by a second set of measurements with displaced temperatures of the isotherms as in [17], or covered by back-extrapolation. This handling of measurement of heat capacity under conditions of steady state has led to the above-mentioned precision of better than 1% [6].

If latent heat effects are present in addition to the heat capacity, they can be similarly treated, as long as steady state is maintained during the transition. If the latent heat evolution or absorption occurs rather gradual, i.e., over a wide temperature range, a heat-capacity baseline must be generated to separate the changes due to changes in temperature and composition. Often, however, the latent heat produces a much larger heat flow than C_p and the analysis mode must be modified [3].

For sharper transitions, another limit exists, suitable for the evaluation of the accompanying latent heat, the so-called 'baseline method' [3]. The following assumptions are made for this baseline method for the evaluation of latent heats from transitions over a narrow temperature range:

- Steady state is maintained until the transition begins.
- At the temperature when the transition begins, another steady state is quickly attained. The sample is in this new steady state at the transition temperature until all latent heat is exchanged, while the reference temperature changes with rate, q. The reference temperature should be checked to note how closely this assumption corresponds to reality.
- When the transition is completed, the system is seriously out of steady state, but this final state of the transition is known to occur close to the peak temperature, and the approach to the final steady state can be extracted from the recorded non-steady state amplitudes [3]. Although the actual amplitudes in this last temperature range do not correspond to the actual thermal activity of the sample, the complete integral from the time of loss of the initial to the regaining of the final steady state corresponds under the given conditions to the latent heat of transition *and* the change in enthalpy over the change in temperature that occurred over the integration time [3]. Note, that the heat-flow rate (dQ/dt) must always be integrated over time, not temperature, which is

commonly done by the software of the calorimeter (without that the user has to be aware of it).
- The heat capacity changes negligibly over the whole temperature range from the loss of the initial steady state to the final regaining of steady state after the transition. Although the two methods of separation of latent heat from the heat capacity effect look similar, they are different in their distance from steady state and the approximations made for their use.

The DSC data of Fig. 15 and the TMDSC data of Fig. 8 data with differently deformed pans, as illustrated in Fig. 3, show that the deformations of the pans change the baseline. If steady state can be reached, measurements of C_p and latent heats can be made by proper adjustment of the heat-flow rate amplitude in the standard DSC. Both types of deformation of the pan decrease the measured heat-flow rate in the endothermic direction, i.e., the sample temperature at a given time increases relative to the reference temperature. For the concave bottom of close-to-equal sample and reference masses in Fig. 15, T_s is even larger than T_r. Increase in the mass of the sample pan reduces the sample temperature, as expected, and yields the endothermic heat flow into the sample calorimeter on heating (a negative heat-flow rate in Fig. 15).

To adjust the baseline in case of pan deformation, or any other change in the geometry, such baseline adjustment is only possible with an internal calibration, as shown in Fig. 8. This correction also requires to identify the instant of deformation, as illustrated with Figs 6 and 7. The measurements before deformation can be treated as usual with an external calibration, or internally, if the sample heat capacity is known under the early condition of measurement, as shown in Fig. 5. After deformation, the new baseline must be found by internal calibration as illustrated in Fig. 8.

The analysis by TMDSC, adds frequency and amplitude of modulation as variables to be considered. In addition to the furnace temperature which governs the standard DSC, in the TMDSC of this study, modulation is controlled at the sample-temperature sensor. It is now not easy to recognize steady state during the given modulation frequency and amplitude. The change in the phase lag of the heat-flow rate on deformation is about 0.7 rad as seen in Fig. 7. The data of Table 1 prove that the initial heating of the fibers and the other measurements on premelted-fibers and PE15520 showed no problems with the analyses, connecting the difficulties to the pan deformation. Table 2 proves that the sample temperature modulation did not deviate from the program in any of the chosen frequencies, i.e., T_s did not lag at the point of its measurement. Furthermore, Table 3 illustrates that the heat-flow-rate response to sinusoidal temperature modulation was truly sinusoidal, so that the erroneous reversing, apparent C_p could not originate from higher harmonics in the response. Based on these observations, Fig. 5 suggests with Eq. (1) that a decrease in heat-flow-rate has caused the decreased C_p. In other words, the sample did not reach the temperature indicated by T_s. Instead of the deformation causing an increasing T_s in standard DSC, in TMDSC, the measured T_s was forced to the proper values, but due to the deformation, the sample lags behind T_s.

This leaves as the final point to investigate the multi-frequency studies of Figs 9–14. First, one can see from a comparison of the two instruments with largely different responses and with different type of generating the various frequencies that successive runs with different frequencies on different samples and simultaneous analysis with multiple frequencies in a single run give similar results despite the unreproducible deformations shown in Fig. 3. Also, the correction for calorimeter asymmetry cannot be a major cause of the surprising frequency dependence of τ since it was needed only for the 2920® DSC. The heat-flow rate amplitudes in Table 2 are higher at higher frequency, than cross-over, and are lower at lower frequency for the runs with a deformed pan relative to the undeformed one which showed the normal decrease of amplitude with frequency. The data from lower frequency and with an underlying heating rate were fitted in Fig. 8 by a shift of the baseline, and gave then reasonable results. Considering the heat capacity of the empty reference pan to be 20 J K^{-1}, the filled sample pan reaches only 25 J K^{-1} because of the small sample mass (the small mass was chosen to avoid undue pressure in the pan on fusion). Furthermore, it was shown earlier by high resolution infrared thermography inside the DSC furnace [22] that undeformed pans heat close to uniformly on top and bottom. Taking all this evidence of phase lag and reverse frequency dependence of the heat-flow rate, the behavior of the deformed sample pan on TMDSC can be explained as follows: The deformation causes an increased thermal resistance to the heat flow due to the smaller contact of the base of the pan. This causes a larger temperature gradient within the sample pan than in the reference pan, and makes the sample lag more than in an undeformed pan. Due to these temperature gradients caused by the deformation, it takes less heat flow to reach the modulation of T_s, set as run parameters. At sufficiently high frequency the reference pan will then appear to have the higher C_p, but positive and negative deviations are not distinguished by the evaluation of A_{HF} in Eq. (1), so that the higher heat-flow rate results. At sufficiently low frequency, even the deformed pan can reach steady state and a baseline correction can yield correct heat capacity data as shown.

Conclusions

The presented experiments with deformed pans illustrate that besides the common check of steady state, linearity, and stationarity, it is also necessary to expand the inspection of the sample calorimeter which consists of pan and sample placed on the measuring platform for external temperature measurement and calibrated heat flux. Not only must the necessary inspections of sample mass, condition and placement on the measuring platform be made before and after the run, to exclude effects such as moisture, decomposition and mechanical movement, but in this paper it is shown, that the pans must also be inspected for deformation. Only when all steps have been done properly can one expect the prior reported precision. The importance of these added precautions when performing DSC and TMDSC can be seen in the frequency of research into fibrous samples [23, 24], temperature modulation [25], relaxation in polymers [26], and analysis of polymers to be recycled [27].

Acknowledgements

'The submitted manuscript has been authored by a contractor of the U.S. Government under the contract No. DOE-AC05-00OR22725. Accordingly, the U.S. Government retains a nonexclusive, royalty-free license to publish, or reproduce the published form of this contribution, or allow others to do so, for U.S. Government purposes.'

This work was supported by the Division of Materials Research, National Science Foundation, Polymers Program, Grant # DMR-0312233 and the Division of Materials Sciences, Office of Basic Energy Sciences, U. S. Department of Energy at Oak Ridge National Laboratory, managed by Lockheed Martin Energy Research Corporation for the U. S. Department of Energy, under contract number DE-AC05-00OR22725.

References

1 B. Wunderlich and M. Dole, J. Polym. Sci., 24 (1957) 201.
2 B. Wunderlich and W. H. Kashdan, J. Polym. Sci., 50 (1961) 71.
3 B. Wunderlich, Differential Thermal Analysis. In A. Weissberger and B. W. Rossiter, eds. Physical Methods of Chemistry, Vol. 1, Part V, Chapter 8, pp. 427–500, John Wiley & Sons, Inc., New York, 1971. Updated in: Thermal Analysis, Academic Press, Boston, 1990; and The Basis of Thermal Analysis, in: E. Turi, ed. Thermal Characterization of Polymeric Materials, Academic Press, New York, revised 2nd ed., pp. 205–482, 1997. Furthermore in preparation as: B. Wunderlich, Thermal Analysis of Polymeric Materials, Springer Verlag, Berlin, 2005.
4 B. Wunderlich, J. Phys. Chem., 69 (1965) 2078.
5 A. Mehta, R. C. Bopp, U. Gaur and B. Wunderlich, J. Thermal Anal., 13 (1978) 197.
6 U. Gaur, A. Mehta and B. Wunderlich, J. Thermal Anal., 13 (1978) 71.
7 B. Wunderlich, Y. Jin and A. Boller, Thermochim. Acta, 238 (1994) 277.
8 J. Pak and B. Wunderlich, Thermochim. Acta, 367 (2001) 229.
9 Y. K. Kwon, R. Androsch, M. Pyda and B. Wunderlich, Thermochim. Acta, 367 (2001) 203.
10 M. Pyda, Y. K. Kwon and B. Wunderlich, Thermochim. Acta, 367 (2001) 217.
11 Heat Capacity and Other Thermodynamic Properties of Linear Macromolecules: U. Gaur, H.-C. Shu, A. Mehta and B. Wunderlich, I. Selenium, J. Phys. Chem., Ref. Data, 10 (1981) 89; U. Gaur and B. Wunderlich, II. Polyethylene, ibid., 119; III. Polyoxides, ibid., 1001; IV. Polypropylene, ibid., 1051; V. Polystyrene, ibid., 11 (1982) 313; U. Gaur, S.-F. Lau, B. B. Wunderlich and B. Wunderlich, VI. Acrylic Polymers, ibid., 1065; U. Gaur, B. B. Wunderlich and B. Wunderlich, VII. Other Carbon Backbone Polymers,ibid., 12 (1983) 29; U. Gaur, S.-F. Lau, B. B. Wunderlich and B. Wunderlich, VIII, Polyesters and Polyamides, ibid., 65; U. Gaur, S.-F. Lau and B. Wunderlich, IX. Aromatic and Inorganic Polymers, ibid., 91; M. Varma-Nair and B. Wunderlich, X. Update of the ATHAS 1980 Data Bank, ibid., 20 (1991) 349.
12 B. Wunderlich, Pure Appl. Chem., 67 (1995) 1019.
13 B. Wunderlich, Heat Capacity of Polymers, in S. Z. D. Cheng, Editor, Handbook of Thermal Analysis and Calorimetry, Vol.3, Applications to Polymers and Plastics, Elsevier Science, Amsterdam, pp. 1–47, 2002.
14 W. Hemminger and G. Höhne, Calorimetry, Verlag Chemie, Weinheim, 1984.
15 R. L. Danley, Thermochim Acta, 395 (2003) 201.
16 A. Boller, Y. Jin and B. Wunderlich, J. Therm. Anal., 42 (1994) 307.
17 Y. K. Kwon, A. Boller, M. Pyda and B. Wunderlich, Polymer, 41 (2000) 6237.
18 J. Pak and B. Wunderlich, Thermochim. Acta, 421 (2004) 203.
19 J. Pak and B. Wunderlich, Macromolecules, 34 (2001) 4492.
20 R. Androsch, I. Moon, S. Kreitmeier and B. Wunderlich, Thermochim. Acta, 357 (2000) 267.
21 T. Ozawa, Bull. Chem. Soc. Japan, 39 (1966) 2071.
22 R. Androsch, M. Pyda, H. Wang and B. Wunderlich, J. Therm. Anal. Cal., 61 (2000) 661.
23 J. F. Turner, A. Riga, A. O'Connor, J. Zhang and J. Collis, J. Therm. Anal. Cal., 75 (2004) 256.
24 A. O'Connor, A. Riga and J. F. Turner, J. Therm. Anal. Cal., 76 (2004) 455.
25 A. Genovese and R. A. Shanks, J. Therm. Anal. Cal., 75 (2004) 233.
26 M. Kattan, E. Dargent and J. Grenet, J. Therm. Anal. Cal., 76 (2004) 379.
27 M. V. L. Fook, A. G. Souza, M. F. S. Trindade, M. M. Conceição, J. C. O. Santos, S. Prasad, V. J. Fernandes Jr. and S. C. L Crispim, J. Therm. Anal. Cal., 75 (2004) 513.

DOI: 10.1007/s10973-005-6805-6